

Fourier-domain optical coherence tomography: next step in optical imaging

MACIEJ WOJTKOWSKI, ANDRZEJ KOWALCZYK, PIOTR TARGOWSKI, IWONA GORCZYŃSKA

Institute of Physics, Nicholas Copernicus University, ul. Grudziądzka 5/7, 87-100 Toruń, Poland.

A new implementation of Fourier domain optical coherence tomography (FDOCT) – a method for imaging the in-depth structure of weakly absorbing and weakly scattering objects is demonstrated. By the reconstruction of both amplitude and phase it is possible to use negative and positive optical path differences to get images of objects of considerable thickness. This method eliminates parasitic autocorrelation terms inherently associated with FDOCT technique and improves the quality of images. The method, experimental set-up, data processing and applications for biomedical imaging are discussed and compared with the time domain version of optical coherence tomography.

1. Introduction

The name “optical tomography” refers to two modalities based on different physical concepts. Both techniques provide a non-contact and non-invasive method of imaging and offer a new attractive tool for medical imaging. In the first method, the density of photon flux created by a modulated source in multiply scattering media or femtosecond pulse propagation are analysed in order to unravel objects embedded in opaque media [1]. Unfortunately, the reconstruction of the spatial distribution of optical parameters within a measured object remains a difficult experimental and theoretical problem which makes this method less disseminated than the second one – the optical coherence tomography (OCT). OCT registers partially coherent light reflected back at discontinuities of the refractive index between tissue layers in the medium that is weakly absorbing and weakly scattering. It uses interferometry in order to measure optical distances between these discontinuities along the penetrating beam. There are two implementations of OCT. In the time domain version, which was historically the first [2], the depth information is obtained by introducing a variable delay into a path of a reference beam. The Fourier domain optical coherence tomography (FDOCT) systems were developed later [3]. In FDOCT the axial information is derived from spectral fringes and this method does not require an optical delay line. A transversal scan of the probing beam provides a 2D section of the investigated structure in both methods.

OCT has been developed during the last decade of the twentieth century and has become an important diagnostic technique in medicine. The most advanced

application of OCT is in ophthalmology. This technique provides high resolution images of the tissue sections of high sensitivity, with precision and in a non-contact and non-invasive way. The 2D scans can be performed either as the images of the sections perpendicular to the tissue surface or as en-face scans at given depths [4], [5].

The next step in the application of OCT is the development of functional OCT. It is realized with spectroscopically sensitive techniques by obtaining absorption spectrum of a tissue at the given depth [6], [7]. OCT combined with Doppler phenomenon demonstrates the ability to quantitative blood flow imaging [8]. The polarization-sensitive OCT detects changes induced in the polarisation state of light that is reflected from the birefringent sample such as muscle, retina and enhance contrast and specificity in identifying structures [9], [10].

An important issue as far as medical applications are concerned is an acquisition time of tomograms. Short acquisition time reduces patients' discomfort, as well as image-blurring motion artifacts. High-speed scanning allows also to obtain the real time acquisition which makes it possible to select the best moment, as well as the best area of interest, to perform a tomogram and to produce video-rate 2D tomograms displaying dynamical processes, like pulsation of blood vessels or movements of plaques attached to a vessel wall. The acquisition speed depends on the time required for a single axial scan. In time-domain OCT it is equal to the time required for the delay line to scan the depth range. Recently, fast delay lines consisting of a grating, a lens, and a galvo-mounted mirror have been developed. Such assemblies produce an axial scan of up to 3 mm depth with the scanning rate of 4 kHz [11]. Another solution is a rotating glass cube which produces an axial scan with velocity of 21 m/s over a range of 3 mm and repetitiveness of 384 Hz [12]. Fast delay lines suffer from nonlinearity problems and the data have to be post-processed [13]. In contrast, Fourier-domain OCT by principle does not require a delay line at all and, therefore, the spectrum measurement is very fast. Further shortening of the acquisition time is achieved by the parallel detection via the so-called smart pixel detector arrays. It eliminates the transversal scan and makes it possible to perform video-rate 3D tomograms [14].

FDOCT has attracted less attention than the well-known time-domain version, notwithstanding its advantages, among others direct access to spectral information [7] and elimination of an optical delay line for depth scanning [15]. The reason was that the image obtained by FDOCT was inherently disturbed by artefacts. In the present contribution we are giving an overview of the basic principles of both time-domain and Fourier-domain OCT and showing how the artifacts inherent in the FDOCT can be overcome.

2. Basic principles

The basic technique of the OCT is partial coherence interferometry. A beam originating from a light source of spectral distribution $S(\nu)$ is split into two partially

coherent beams. One beam penetrates the object along the z -axis, and is reflected back from the n -th layer. The field spectral component of this beam has a form

$$U_n(\nu) = b_n S(\nu) \exp(-2\pi i \nu (t + 2\tau_n)) \tag{1}$$

where b_n is the reflectivity coefficient which, we assume, is independent of ν . A second beam is reflected from the reference mirror

$$U_r(\nu) = b_r S(\nu) \exp(-2\pi i \nu (t + 2\tau_r)). \tag{2}$$

The above two beams are delayed by $2\tau_n$ and $2\tau_r$, where delay times $\tau_{n,r} = z_{n,r}/c$ are related to the location of each reflecting layer (z_n) and the position of the reference mirror (z_r), respectively. These two fields are added and time-averaged in the interferometer, and the final steady-state intensity spectrum $G_{UU}(\nu)$ has the following form:

$$\begin{aligned} G_{UU}(\nu) &= \left| U_r(\nu) + \sum_n U_n(\nu) \right|^2 = G_{rr}(\nu) + \sum_n G_{nn}(\nu) \\ &+ 2\text{Re} \left\{ \sum_{n \neq m} G_{nm}(\nu) \exp(-2\pi i \nu (\tau_n - \tau_m)) \right\} \\ &+ 2\text{Re} \left\{ \sum_n G_{nr}(\nu) \exp(-2\pi i \nu (\tau_n - \tau_r)) \right\} \end{aligned} \tag{3}$$

where

$$G_{mn}(\nu) \equiv b_n b_m \lim_{T \rightarrow \infty} \left[\frac{S(\nu) S^*(\nu)}{2T} \right]$$

is proportional to the steady spectrum of the source.

The first two terms of Eq. (3) are intensities from the reference mirror and scattering centres within the object. The next term is parasitic (the so-called autocorrelation) and is associated with the mutual interference of all elementary waves scattered within the object. The last term contains direct information on the positions of scattering centres along the penetration beam with respect to the constant position of the reference mirror.

According to the Wiener-Khinchin theorem [16], there is a correspondence between the spectral density function $G(\nu)$ and the complex first-order electric field correlation function

$$\Gamma(\tau) = \text{FT}^{-1} \{ G(\nu) \}. \tag{4}$$

The total signal, as registered by a photodiode, is represented by Eq. (3) integrated over the whole spectral band

$$I(\tau_r) = \Gamma_{rr}(0) + \sum_n \Gamma_{nn}(0) + 2 \sum_{n \neq m} \Gamma(\tau_m - \tau_n) + 2 \sum_n \Gamma(\tau_r - \tau_n). \tag{5}$$

If τ_r is scanned by introducing a variable optical delay line into a reference beam, the first three terms will provide a constant background. The last one will produce an interference effect when the path length in the reference and object arms of the interferometer are matched within the correlation length of the light, *i.e.*, when $\tau_r = \tau_n$ (time-domain OCT).

An alternative method is to split the total signal into spectral components by a spectrograph, register the spectrum and perform the Fourier transform numerically (FDOCT). The inverse Fourier transformation of Eq. (3), taking into account Eq. (4), yields

$$\begin{aligned} \text{FT}^{-1}\{G_{UU}(v)\} = & \Gamma_{rr}(\tau) + \sum_n \Gamma_{nn}(\tau) + \sum_{n \neq m} \Gamma(\tau + (\tau_m - \tau_n)) + \sum_{n \neq m} \Gamma(\tau - (\tau_m - \tau_n)) \\ & + \sum_n \Gamma(\tau + (\tau_r - \tau_n)) + \sum_n \Gamma(\tau - (\tau_r - \tau_n)). \end{aligned} \quad (6)$$

Due to the fact that spectral density is a real function, and its Fourier transform is Hermitian, the Eq. (6) is symmetrical about $\tau = 0$. The signal described in Eq. (6) consists of the terms which will give peaks at following locations: $\tau = 0$ corresponding to the intensities of the reflected reference beam and of beams reflected from the layers distributed within the object, $\tau = \tau_m \pm \tau_n$ associated with the interference of all elementary waves reflected back from different object interfaces, and $\tau = \tau_r \pm \tau_n$ originating from the interference between reflected object waves and the wave reflected from the reference mirror. The last two terms include direct information on the positions of reflecting layers with respect to the constant position of the reference mirror.

Analysis of Eqs. (5) and (6) makes it clear that theoretically both time-domain and Fourier-domain mutations are equivalent. In practice, however, there is a disadvantage of the FDOCT because the four first terms give rise to parasitic terms. Additionally, the symmetry of Eq. (6) causes the unwanted mirror image of reflecting layers. This artefact and a coherent noise obscure the resultant image.

In order to eliminate these shortcomings we have applied a five-frame method adopted from the field of digital holography [17] which allows reconstructing the complex form of the last term in Eq. (3)

$$\sum_n G_{nr}(v) \exp(-2\pi i v(\tau_n - \tau_r)) \equiv A(v) \exp(i\Phi(v)). \quad (7)$$

From five measurements of the spectra $G_{nb}^{(k)}(v)$ taken with consecutive phase shifts of $\pi/2$ the amplitude $A(v)$ and the phase $\Phi(v)$ are calculated according to the following formulas [17]:

$$A = \frac{1}{4} \sqrt{[2(G^{[2]} - G^{[4]})]^2 + [2G^{[3]} - G^{[5]} - G^{[1]}]^2}, \quad (8a)$$

$$\Phi = \arctan \frac{2(G^{[2]} - G^{[4]})}{2G^{[3]} - G^{[5]} - G^{[1]}} \quad (8b)$$

where

$$G^{[k]} = G_{UV} \left(\Phi(v) + k \frac{\pi}{2} \right),$$

$$k = 1, 2, \dots, 5.$$

Finally, the Fourier transform of the complex function yields

$$\text{FT}^{-1} \{A(v) \exp(i\Phi(v))\} = \sum_n \Gamma(\tau - (\tau_r - \tau_n)), \quad (9)$$

which provides structural information on the object free of parasitical terms as well as of the mirror image. In result, the accessible depth range expands by a factor of two. The price to be paid is fivefold increase in the total acquisition time.

3. Instrument

3.1 General design

A conventional OCT instrument consists of an interferometer, a source of temporally low and spatially high coherent light, a reference mirror, and a detector. The interferometer is usually Michelson type but others, as Mach-Zender [18], are also operating. Both bench-top, open air and portable fiber-optic designs [19] are applied. The most popular light source is a superluminescent diode emitting in a near IR region with a bandwidth of few tens of nanometers. The other alternatives are: rare earth doped fibers [20], mode locked Ti:sapphire lasers [21] and frequency tunable lasers [22].

The reference mirror in time-domain OCT is movable – it has to scan the axial depth. In FDOCT the mirror is either immobile or is mounted on the piezo translator to perform a few (up to five) discrete shifts by a fraction of a light wavelength.

The detector in time domain version is a photodiode which detects time-varying signal during the scan of the delay line in the reference arm. In FDOCT the spectral fringes are produced by a grating and registered by a CCD, then the data are transferred to a PC where the Fourier transform is calculated.

The optics in the object arm has to aim and focus the beam within a sample and perform a transversal scan. The design depends on the location of tissue to be imaged. The simplest is an open air optic rigidly attached to the interferometer. In ophthalmic applications a design should take into account the optics of the eye and the measurement should be possible without pupil dilation. It is also desirable to incorporate the OCT instrument into fundus camera. The hand-held probes connected with fiber OCT systems allow to reach every point on the skin surface. An endoscope [23] allows investigating cavities of the body. In extreme case a video-rate tomograms of cholesterol plaques attached to the blood vessels can be taken by a catheter mounted at the end of the fiber [24].

3.2. Resolution and signal to noise ratio

In both FDOCT and time-domain OCT the resolution of the system depends on the same factors. The resolution in the axial direction depends on the coherence length of the light source, which is inversely proportional to the source bandwidth [25]

$$\delta z = \frac{l_c}{2} = \frac{2 \ln 2}{\pi n_R} \frac{\lambda_0^2}{\text{FWHM}(\lambda)} \quad (10)$$

where λ_0 and $\text{FWHM}(\lambda)$ are the central wavelength and the full width half maximum of the spectrum, respectively, and n_R is the refractive index of the examined medium. The broadening of the source bandwidth has the opposite effect on the coherence length when dispersion is introduced into the system. This may be due to a dispersive object (*e.g.*, the eye) or due to fibers employed in the system. Therefore, in the absence of additional dispersion correcting procedures, there are optimal bandwidths of the source ranging from 26 nm to 83 nm, which produces the best resolution in different parts of the eye [26]. The highest resolution achieved so far is 1 μm in nontransparent tissue and 2–5 μm in the cornea and retina *in vivo* [21]. To obtain such resolution careful dispersion compensation is required.

The resolution in transversal direction is determined by the focusing properties of the optics and is about few tens of micrometer. It can be improved by increasing the aperture of the incident beam. This is achieved by reducing the focal length of the object lens.

The imaging depth can be limited by the spectral resolution of the spectrometer, the focal depth and attenuating properties of the medium. The information about the object structure is deciphered by the numerical fast Fourier transform (FFT) of the measured signal. The number of sampling points N is given by the number of illuminated CCD pixels. The imaging depth of a FDOCT device is [27]

$$l_{\max} = \frac{1}{4n_R} \frac{\lambda_0^2}{\Delta\lambda} N \quad (11)$$

where $\Delta\lambda$ is the width of the spectrum registered by the CCD matrix. If the medium is highly absorbing or scattering, the effective depth can be further reduced.

It must be noted that there is a tradeoff between the focal spot, which determines transversal resolution, and the focal depth. Two concepts were proposed to overcome this limitation. The first is the so-called dynamic focus where the delay and the focal position are changed simultaneously [25]. The second is based on the properties of an axicon lens which is used as an objective into the sampling arm [28]. With the latter the 10 μm transversal resolution with 6 mm focusing depth is obtained.

An important feature of every OCT system, which describes the measurement performance, is a dynamic range. A coherence detection [29] either heterodyne (time-domain OCT) or homodyne (FDOCT) allows to achieve the shot noise limit by an introduction of a reference signal of sufficient intensity, but within a saturation limit of a detector. Under such conditions the dynamic range in FDOCT is given by the

following formula [30]:

$$DR = 10\log\left(\frac{FWC}{2}\right) = 10\log\left(\frac{[Pt]_{\max}\eta}{2Nh\nu}\right) \tag{12}$$

where FWC is the full-well capacity of the CCD, P – the optical power from the object, t – the exposure time, $[Pt]_{\max}$ – the saturation energy of N illuminated pixels, η – the quantum efficiency, h – the Planck constant and ν is the central frequency of the incident light wave. The Fourier transformation of the signal acts as a narrow band-pass filter [31]: let us assume the axial point spread function equals k pixels – it means that the Fourier transformation is “compressing” information of the harmonic function into k pixels. Since the white noise is distributed after FFT equally over $N/2$ pixels, the maximum signal to noise ratio is increased by factor $(N/2)/k$

$$DR = 10\log\left(\frac{FWC N}{4k}\right) \tag{13}$$

3.3. Fourier-domain OCT instrument

Our FDOCT system (Fig. 1) is based on a Michelson interferometer set-up. A superluminescent diode (Superlum – Moscow, $\lambda = 810$ nm, 20 nm FWHM, maximal output power of 2 mW) is a light source of low temporal but high spatial coherence. The detection unit consists of a diffraction grating (1800 grooves/mm Spectrogon) and a 18-bit cooled CCD camera (Andor Technologies, 1 MHz sampling rate of a frame grabber, 16 bit AD conversion, 1024×128 pixels, 27×27 μm pixel size, full vertical binning). In order to introduce phase shifts (needed

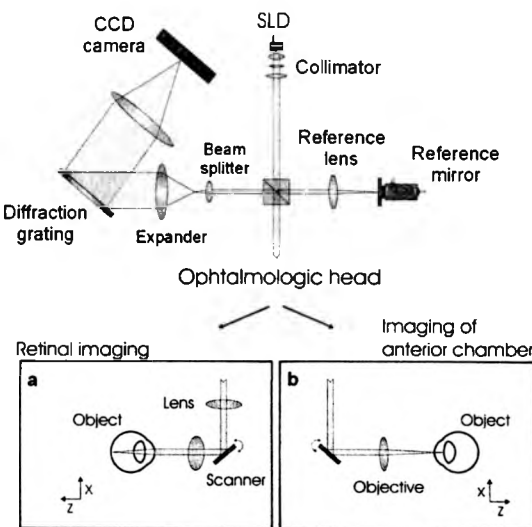


Fig. 1. Optical scheme of the Fourier-domain spectral OCT device (SLD – superluminescent diode).

for the five-frame FDOCT) into the reference beam, the mirror is mounted on a piezo-translator (Physik Instrumente).

The optics in the object arm is designed to achieve retinal imaging without pupil dilation. A parallel beam, which illuminates the cornea, is eventually focused by the eye optics onto the retina. The pivot of the transverse scanner is imaged in the plane of the patient's pupil by the lens. Such arrangement provides maximal scanning range for a given objective aperture (Fig. 1a). When the tomogram of the anterior chamber is taken, the transverse scanner and the cornea are placed at the focal points of the object lens (Fig. 1b). Such set-up ensures that the direction of the beam is insensitive to the scanner angle. This system scans the object in linear fashion and is used for skin imaging as well.

The imaging depth in our FDOCT equals approximately 3.5 mm. It is sufficient to make tomograms of the anterior chamber. It is reduced either by penetration depth or (as in the case of retina) properties of the optical system of the eye.

The shot noise level in our system is easily reached [32] due to the inherently low dark and read noise figures of CCDs. This fact can be also demonstrated experimentally by switching off the camera cooling system – the increase in thermal noise does not deteriorate the FDOCT image quality. Assuming parameter $k = 2$, the theoretically estimated value for the DR (Eq. (13)) in our system equals 79 dB. We experimentally determined the dynamic range to be 67 dB. The application of the five-frame method reduces the noise level by 7.5 dB and finally the dynamic range of the five-frame FDOCT method is in our case 74 dB.

4. Experimental results

Figure 2 presents a comparison between two tomograms of a hard contact lens placed on the rabbit cornea *in vitro* obtained with the standard and five-frame FDOCT techniques. Parasitic terms typical of the standard FDOCT technique are clearly demonstrated in Fig. 2a. The autocorrelation terms are strongest for small

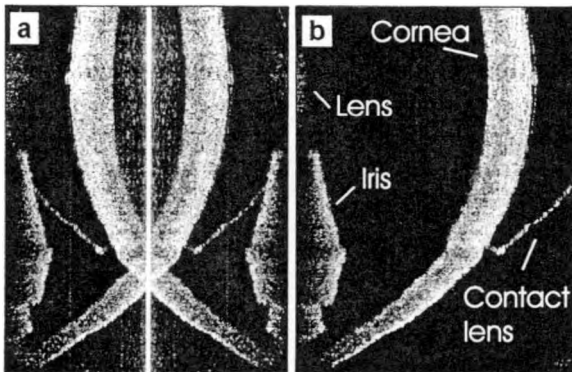


Fig. 2. Optical tomograms of a hard contact lens positioned on the rabbit eye *in vitro*. a – standard FDOCT, b – five-frame FDOCT.

fringes frequencies, *i.e.*, close to the zero path difference (central white stripe). However, even for longer optical distances one can still observe some autocorrelation terms (regular vertical stripes) originating from the interference between the rays reflected back from different optical components in the instrument. The superimposed mirror image is due to the fact that a real function (spectrum) is an argument of the Fourier transform. The five-frame technique efficiently reduces these all artifacts and uncovers the details of the sample (Fig. 2b). One can note that the geometrical contours of the contact lens are very sharp due to the abrupt change in the refractive index between air and the contact lens. The useful depth range doubles to 0.4 cm. The cornea, iris, lens and some post-mortem changes in eye structure are clearly visible. There is no scattered back signal from the volume of the contact lens because the material is homogenous. In contrast, the cornea has fibrous structure and therefore there is a measurable signal originating from the light scattered back from its structure. The axial resolution may be judged by the visible gap between the contact lens and the retina which is estimated as 25 μm .

In the following experiments we tested the possibility of using the FDOCT technique in imaging the strongly scattering media. For the retina and the skin the penetration depth was about 1 mm. Because the resulting images were thin there was no need for five-frame method and the measurements were performed with the aid of the standard FDOCT technique.

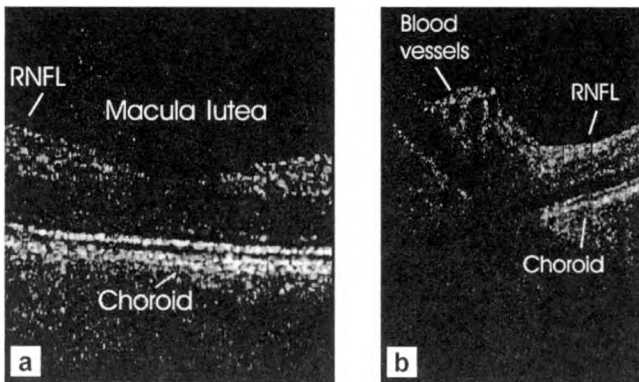


Fig. 3. Optical tomograms of human retina *in vivo* taken by a standard FDOCT. a – macula lutea, b – peripheral part of the human optic disc with visible blood vessels.

To demonstrate the potential use of FDOCT for the imaging of the human retina *in vivo* (Fig. 3a,b) we examined the left eye of a volunteer (K.W., 27 years, female, healthy eye). It is worthwhile to note that the measurement took place without dilation of the iris and the optics of the eye was an inherent part of the sample arm of the interferometer. The region of the central retina around the *macula lutea* is presented in Fig. 3a. The surface topology with details of foveal pit and the retinal interfaces, RNFL – retinal nervous fiber layer and choroid, can be easily identified [33], [34]. A topography of the human peripheral part of an optic disc section,

as well as a retinal structure in its vicinity, is displayed in Fig. 3b. Concentration of blood vessels in this region is very high; they are visible as oval structures in Fig. 3b.

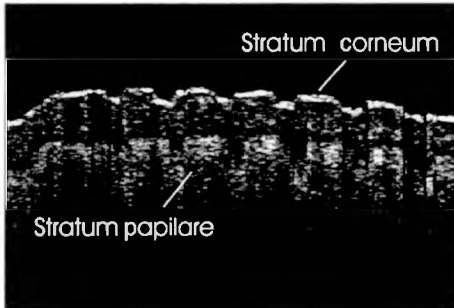


Fig. 4. Optical tomogram of the skin from an internal part of the thumb taken by standard FDOCT.

An example of an image of the human skin is given in Fig. 4. The light penetrates to about 1 mm below the surface and provides images only to the depth of the papillary layer of the dermis. Nevertheless, it could be satisfactory for cosmetic applications. Optimisation of the wavelength may extend the penetration depth up to 3 mm [35].

5. Discussion

We demonstrated the possibilities of morphological ophthalmologic imaging with the aid of the modified FDOCT technique. It was shown that five-frame FDOCT produces images which are free of parasitic autocorrelation terms, the only drawback being five-fold increase in the acquisition time. For the 16 bit CCD system in use, the data transfer of 1024 spectral points to the personal computer needed 4 ms. Hence, with FDOCT we need approximately 20 ms for one optical A-scan. The total five-frame FDOCT tomographic image of 256 axial scans takes about 5 s, which is, however, acceptable as far as an examination of a patient is concerned.

The saturation level of CCD detector is many orders of magnitude lower than for photodiodes. Therefore, for time-domain OCT systems the calculated values of above 100 dB were reported [30], [36], much more than 79 dB obtained in the present contribution. Despite this considerable difference the quality of the presented retinal tomograms obtained by FDOCT are not much worse than the best time-domain OCT retinal images [37]. This apparent contradiction may be explained by the fact that the dynamic range that is necessary to distinguish between retinal layers essential for ophthalmologic diagnosis is approximately equal to 40 dB [38], which fits well to the dynamic range of our FDOCT system.

The benefits of the presented method are: the absence of overlapping mirror images, the extended depth range, higher signal to noise ratio and simple

interpretation of thick biological samples. The price to be paid is a five-fold increase in the measurement time. The next disadvantage is that the presented method requires high stability of an object. The object displacement as small as $\lambda/10$ during a five-frame cycle completely precludes the faithful reconstruction. Therefore, in order to perform *in vivo* measurements the system has to collect all five spectra simultaneously.

OCT provide us with optical distance of reflecting layers along the probing beam. To obtain the geometrical distances one has to divide the optical distances by the group index of refraction for each region. Additionally, for oblique incidence, one has to take into account refraction on the borders of these regions and correct the image if an exact geometrical image is required [13].

In conclusion, we have demonstrated that images produced by FDOCT produced appear competitive to those obtained by conventional OCT instruments that are based on a time-domain measurement set-up.

Acknowledgments – The authors are grateful for financial support from the State Committee for Scientific Research (KBN), Poland (Grant No. 4T11E023 22).

References

- [1] MINET O., MÜLLER G., BEUTHAN J., [Eds.], *Selected Papers on Optical Tomography – Fundamentals and Applications in Medicine*, SPIE Milestone Series, Vol. 147, Washington 1998.
- [2] HUANG D., SWANSON E.A., LIN C.P., SCHUMAN J.S., STINSON W.G., CHANG W., HEE M.R., FLOTTE T., GREGORY K., PULIAFITO C.A., FUJIMOTO J.G., *Science* **254** (1991), 1178.
- [3] FERCHER A.F., HITZENBERGER C.K., KAMP G., EL-ZAIAT S.Y., *Opt. Commun.* **117** (1995), 43.
- [4] HAÜSLER G., LINDNER M.W., *J. Biomed. Opt.* **3** (1998), 21.
- [5] ROGERS J.A., PODOLEANU A. G., DOBRE G.M., JACKSON D.A., FRITZKE F.W., *Opt. Express* **9** (2001), 533.
- [6] MORGNER U., DREXLER W., KÄRTNER F.X., LI X.D., PITRIS C., IPPEN E.P., FUJIMOTO J.G., *Opt. Lett.* **25** (2000), 111.
- [7] LEITGEB R., WOJTKOWSKI M., HITZENBERGER C.K., STICKER M., KOWALCZYK A., FERCHER A. F., *Opt. Lett.* **25** (2000), 820.
- [8] DING Z., ZHAO Y., REN H., NELSON J.S., CHEN Z., *Opt. Express* **10** (2002), 236.
- [9] PARK B.H., SAXER C., SRINIVAS S.M., NELSON J.S., DE BOER J.F., *J. Biomed. Opt.* **6** (2001), 474.
- [10] HEE M.R., HUANG D., SWANSON E.A., FUJIMOTO J.G., *J. Opt. Soc. Am. B* **9** (1992), 903.
- [11] ROLLINS A.M., KULKARNI M.D., YAZDANFAR S., UNG-ARUNYAWEE R., IZATT J.A., *Opt. Express* **3** (1998), 219.
- [12] BALLIF J., GIANOTTI R., CHORANNE P., WÄLTI R., SALATHÉ R.P., *Opt. Lett.* **22** (1997), 757.
- [13] WESPHAL V., ROLLINS A., RADHAKRISHNAN S., IZATT J.A., *Opt. Express* **10** (2002), 397.
- [14] LAUBSCHER M., DUCROS M., KARAMATA B., LASSER T., SALATHÉ R., *Opt. Express* **10** (2002), 429.
- [15] ZULUAGA A.F., RICHARDS-KORTUM R., *Opt. Lett.* **24** (1999), 519.
- [16] GOODMAN J.W., *Statistical Optics*, Wiley, New York 1985.
- [17] SCHMIT J., CREATH K., *Appl. Opt.* **34** (1995), 3610.
- [18] MASTERS B.S., [Ed.], *Selected Papers in Optical Coherence Interferometry & Tomography*, SPIE Milestone Series, Vol. 165, Washington 2001.
- [19] PODOLEANU A.G., SEEGER M., DOBRE G.M., WEBB D.J., JACKSON D.A., FRITZKE F.W., *J. Biomed. Opt.* **3** (1998), 12.
- [20] BOUMA B.E., NELSON L.E., TEARNEY G.J., JONES D.J., BREZINSKI M.E., FUJIMOTO J.G., *J. Biomed. Opt.* **3** (1998), 76.

- [21] DREXLER W., MORGNER U., KÄRTNER F.X., PITRIS C., BOPPART S.A., LI X.D., IPPEN E.P., FUJIMOTO J.G., *Opt. Lett.* **24** (1999), 1221.
- [22] HABERLAND U.H.P., BLAZEK V., SCHMITT H.J., *J. Biomed. Opt.* **3** (1998), 259.
- [23] TEARNEY G.J., BREZINSKI M.E., BOUMA B.E., BOPPART S.A., PITRIS C., SOUTHERN J.F., FUJIMOTO J.G., *Science* **276** (1997) 2037.
- [24] PATWARI P., WEISSMAN N.J., BOPPART S.A., JESSER CH., STAMPER D., FUJIMOTO J.G., BREZINSKI M.E., *Am. J. Cardiol.* **85** (2000), 641.
- [25] FERCHER A.F., *J. Biomed. Opt.* **1** (1996), 157.
- [26] HITZENBERGER C.K., DREXLER W., BAUMGARTNER A., FERCHER A.F., *Proc. SPIE* **2981** (1997), 29.
- [27] WOJTKOWSKI M., LEITGEB R., KOWALCZYK A., BAJRASZEWSKI T., FERCHER A.F., *J. Biomed. Opt.* **7** (2002), 457.
- [28] DING Z., REN H., ZHAO Y., NELSON J.S., CHEN Z., *Opt. Lett.* **27** (2002), 243.
- [29] SALEH B.E.A., TEICH M.C., *Fundamentals of Photonics*, Wiley, New York 1991.
- [30] SWANSON E.A., IZATT J.A., HUANG D., HEE M.R., FUJIMOTO J.G., LIN C.P., PULIAFITO C.A., *Opt. Lett.* **17** (1992), 151.
- [31] DREXLER W., HITZENBERGER C.K., SATMANN H., FERCHER A.F., *Opt. Eng.* **34** (1995), 701.
- [32] *Catalogue Oriel Instruments: New Multichannel Detection Systems*, 1988, pp. 2–5.
- [33] TOTH C.A., NARAYAN D.G., BOPPART S.A., HEE M.R., FUJIMOTO J.G., BIRNGRUBER R., CAIN C.P., DiCARLO C.D., ROACH W.P., *Arch. Ophthalmol.* **115** (1997), 1425.
- [34] BAUMGARTNER A., HITZENBERGER C.K., SATMANN H., DREXLER W., FERCHER A.F., *J. Biomed. Opt.* **3** (1998), 45.
- [35] DE BOER J.F., SRINIVAS S.M., MALEKAFZALI A., CHEN Z., NELSON J.Z., *Opt. Express* **3** (1998), 212.
- [36] WANG X.J., MILLNER T.E., NELSON J.S., *Opt. Lett.* **20** (1995), 1337.
- [37] DREXLER W., GHANTA R.K., SCHUMAN J.S., KO T., MORGNER U., KÄRTNER F.X., FUJIMOTO J.G., *Proc. SPIE* **4251** (2001), 183.
- [38] PULIAFITO C.A., HEE M.R., LIN C.P., REICHEL E., SCHUMAN J.S., DUKER J.C., IZATT J.A., SWANSON E.A., FUJIMOTO J.G., *Ophthalmol.* **102** (1995), 217.

Received July 12, 2002